Available online at www.sciencedirect.com
SCIENCE DIRECT
International Journal of Heat and Mass Transfer 49 (2006) 3601–3616
International Journal of HEAT and MASS TRANSFER
www.elsevier.com/locate/ijhmt

Numerical study of the influence of a longitudinal sound field on natural convection in a cavity

Hong Lei, Daniel Henry *, Hamda BenHadid

Laboratoire de Mécanique des, Fluides et d'Acoustique, UMR CNRS 5509, Ecole Centrale de Lyon/Université Claude Bernard Lyon 1/INSA de Lyon, ECL, 36 avenue Guy de Collongue, 69134 Ecully Cedex, France

Received 13 June 2005; received in revised form 5 February 2006
Available online 27 April 2006

Abstract

Numerical experiments have been performed in order to investigate the convection in an enclosure of aspect ratios 5:1:1.3 subject to a horizontal temperature gradient and a longitudinal sound field. The governing equations are solved by a spectral element method. Different flow structures appear when increasing (or decreasing) the Grashof number. Without acoustic field (acoustic Froude number $Fr = 0$), a hysteresis occurs connected to a first steady bifurcation with breaking of symmetry, but for $Fr \neq 0$, no hysteresis is observed as this symmetry is no more effective. The further transition to oscillatory flow is found to be stabilized by the acoustic field. Depending on Fr, this transition can occur with or without the breaking of the left–right symmetry.

Keywords: Rayleigh streaming; Standing wave; Thermal convection; Hysteresis; Bifurcation

1. Introduction

It is now well known that a steady vortex flow can be induced by sound wave propagation through a fluid. This effect is called acoustic streaming. There are two types of acoustic streaming: Eckart streaming and Rayleigh streaming [1,2]. In the former, the Reynolds stresses arise within the main body of the fluid when an ultrasonic beam propagates into it. In the latter, the stresses act in the Stokes shear-wave layer that forms at a solid boundary. Extensive studies have been carried out to study Eckart streaming. But there are fewer studies about Rayleigh streaming, mainly experiments and analytic studies, and very few numerical studies already considered the coupled effect of Rayleigh streaming and thermal convection, despite its interest for applications on the control of thermally induced flows and heat transfers.

In 1848, Rayleigh was the first to analytically study the streaming pattern when a standing wave is applied between two parallel plates [3]. For this type of acoustic streaming, the flow, originated in the Stokes layer, is due to the interaction between the inertia and viscosity forces, but the magnitude of the velocity is independent of the viscosity [4,5].

Some researchers experimentally studied the Rayleigh streaming and its effect on natural convection. Concerning Rayleigh streaming alone, Arroyo [6] used particle image velocimetry and stereoscopy to measure the three-dimensional velocity field caused by acoustic waves. He obtained good comparisons between the measured boundary velocity and that deduced through a model from pressure measurements. Campbell [7] reviewed the application of laser Doppler anemometry and particle image velocimetry to the measurement of acoustic streaming, and gave the velocity map generated by acoustic streaming. Concerning the effect on natural convection, Richardson [8] used the shadowgraph technique to observe a heated horizontal circular cylinder subjected to transverse horizontal or vertical sound fields. The observations confirmed the local changes in

* Corresponding author. Tel.: +33 4 72 18 61 70; fax: +33 4 78 64 71 45.
E-mail addresses: cn_leihong@yahoo.com (H. Lei), daniel.henry@eclyon.fr (D. Henry).

0017-9310/$ - see front matter © 2006 Elsevier Ltd. All rights reserved.
doi:10.1016/j.ijheatmasstransfer.2006.02.045

Nomenclature

A	amplitude for the bifurcation diagrams
A_x	aspect ratio along the longitudinal x direction
A_z	aspect ratio along the transverse z direction
c_0	speed of sound
$\mathrm{d}s$	elementary surface
$\mathrm{d}v$	elementary volume
e_y	unit vector of the y reference axis
F	force
Fr	acoustic Froude number
g	gravity
Gr	Grashof number ($Gr = \beta g \Delta \bar{T} H^3/(A_x \nu^2)$)
Gr_{old}, Gr_{new}	successive values of Gr used in the computations
H	height of the cavity (along y)
$k = \omega/c_0$	wave number of the sound wave
L^*	characteristic length
L	length of the cavity (along x)
n	superscript indicating the time step
Nu	Nusselt number
p	dimensionless pressure
p_1	amplitude of the acoustic pressure
P_{xy}, P_{xz} and P_{yz}	principal middle planes
Pe	Peclet number
Pr	Prandtl number ($Pr = \nu/\kappa$)
Re	Reynolds number
R_{s}	streaming Reynolds number
$\hat{R}_{\mathrm{s}}$	streaming Reynolds number defined by Stuart [18]
$\hat{\hat{R}}_{\mathrm{s}}$	streaming Reynolds number defined by Vainshtein [14,16]
S	symmetry with respect to P_{xy} plane (left–right symmetry)
S_{r}	π rotational symmetry about the z'-axis
Surf	transverse section of the cavity
t	time
T	dimensionless temperature
T_{c}	dimensionless temperature imposed at the left cold wall
T_{h}	dimensionless temperature imposed at the right hot wall
$\bar{T}_{\mathrm{c}}$	temperature imposed at the left cold wall
$\bar{T}_{\mathrm{h}}$	temperature imposed at the right hot wall
T_{fm}	mean fluid temperature
U^*	characteristic velocity
$\vec{V}$	dimensionless fluid velocity vector
$V_x = u$, $V_y = v$ and $V_z = w$	components of the dimensionless fluid velocity
$v_0 = \frac{3V_0^2}{8c_0}$	amplitude of the steady slip velocity
V_0	amplitude of V'
V_s	steady slip velocity generated by the acoustic wave
V'	velocity fluctuation due to the acoustic standing wave
Vol	volume of the cavity
W	width of the cavity (along z)
x, z	horizontal reference axes
y	vertical reference axis
z'	middle transverse axis parallel to z

Greek symbols

β	thermal expansion coefficient of the fluid
$\delta = \sqrt{\frac{2\nu}{\omega}}$	acoustic boundary layer
ΔGr	step in Gr
$\Delta \bar{T} = (\bar{T}_{\mathrm{h}} - \bar{T}_{\mathrm{c}})$	applied temperature difference
κ	thermal diffusivity of the fluid
λ	sound wavelength
∇	nabla operator
ν	kinematic viscosity of the fluid
ω	angular frequency of the sound wave
$\frac{\partial}{\partial n}$	normal derivative
ρ	fluid density
ρ_0	reference fluid density
θ	dimensionless time
ε	maximum variation between time steps
ε_0	criterion for steady state convergence

boundary layer thickness and heat transfer, and provided new evidence of the progressive splitting of the rising plume with a horizontal sound field. Matsumura [9] investigated the influence of a sound field on the natural convective heat transfer from vertical flat plates, and indicated that the width of the plates and the frequency of the sound waves played an important role on heat transfer. Engelbrecht [10] studied the influence of acoustic waves on the transition from laminar to turbulent flow in the boundary layer along a heated vertical flat plate, and gave the relationship between the sound frequency at which transition occurred and the critical Grashof number. Kawahara [11] used a CCD camera to measure the evolution of the surface shape of a sphere layered with a volatile solid substance and submitted or not to an ultrasonic acoustic field (levitation purpose). They indicated a major influence of acoustic streaming on sublimation for strong acoustic fields. Based on the steady state technique, Gopinath [12] measured the convective heat transfer from a heated cylinder in an intense acoustic field, and identified two distinct flow regimes. One is the laminar attached flow regime which shows the expected square root dependence of the Nusselt number. Another is an unstable regime in which vortex shedding is prevalent, contributing to higher heat transfer rates.

Some theoretical works were also carried out to study the fluid flow and the heat transfer caused by the sound field. Starting from the Navier–Stokes equations, Westervelt [5] obtained a general equation governing the

generation of vorticity. A specialization of the vorticity equation to the case of solenoidal first-order motion leads to the generating term employed by Rayleigh and Schlichting, and a specialization to the case of irrotational first-order motion leads to the generating term employed by Eckart. De Vahl Davis [13] considered the influence of acoustic field on buoyancy and pointed out that horizontal oscillations increased heat transfer at the bottom of a cylinder and vertical oscillations decreased the local heat transfer. Vainshtein [14–16] studied the acoustic streaming and its effect in different situations. We can mention the theoretical analysis of the effect of acoustic standing waves on the heat transfer between plates. Relationships were derived between the averaged Nusselt number and the acoustic Peclet number Pe for the cases of $Pe \gg 1$ and $Pe \ll 1$. Chu [17] studied the stability of acoustic streaming flow induced by a small-amplitude surface acoustic wave propagating along the walls of a confined parallel-plane channel, and indicated that the critical Reynolds number was smaller than that for conventional pressure driven flows.

The present work is connected to the technologies of materials processing (semi-conductors and metallic compounds such as InP, GaAs, In–Sb, Bi–Sb, In–Cd,...) by directional solidification from their melt. In such processes, the control of the fluid motions induced in the melt is particularly important and it has then been a main research objective for the last decade. In this context, the use of ultrasound waves is a new promising tool which has already been shown to be efficient in solidification situations, inducing a clear decrease of the concentration segregation as mentioned by Kozhemyakin et al. [18,19]. Our work will refer to the horizontal Bridgman crystal growth configuration with a low Prandtl number fluid ($Pr = 0.019$, Gallium compounds). We will deal with the influence of the Rayleigh acoustic streaming on buoyancy driven flows in a parallelepipedic side-heated cavity. We will focus on the transition to oscillatory flows which is known as the threshold for changes of behaviours, as better heat transfer and mixing but worse conditions for material processing. The major concern of our numerical work is to study the evolution of the flow under different sound fields, to document and discuss the bifurcations that occur as the Grashof number is progressively either increased or decreased, and to investigate the structure of the flows and the changes in heat transfer. These results are presented and discussed in the following, after the presentation of the mathematical model and the numerical methods.

2. Mathematical model

The study focuses on the convective flow in a rectangular enclosure similar to that used in the experiment of Hof et al. [20] on the flow damping by magnetic field. The aspect ratios of the enclosure (A_x,1,A_z) are 5:1:1.3, corresponding to dimensionless length (L), height (H) and width (W), respectively, H being chosen as the reference length. Constant uniform temperature $\bar{T}_h$ and $\bar{T}_c$ (with $\bar{T}_h > \bar{T}_c$) are imposed at the right and left walls, respectively. The other walls are assumed to be adiabatic. The standing wave acoustic field is also applied in the horizontal direction, and satisfies $\lambda = 4L$, where λ is the acoustic wavelength. The orthogonal reference axes are x, y and z, and z' axis is also introduced to describe the flow field, as shown in Fig. 1.

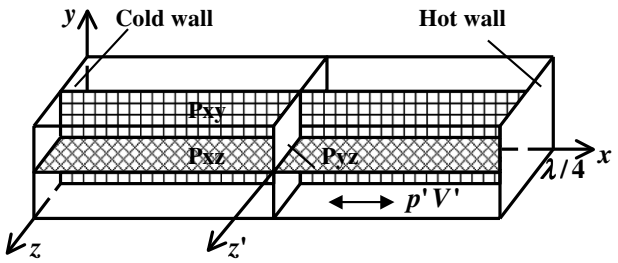

Fig. 1. Schematic diagram of the studied situation and coordinate system.

2.1. Acoustic streaming model

Let us consider the Reynolds acoustic streaming based on a standing plane wave in the x direction. With the classical assumptions for sound propagation, the velocity fluctuation V' due to the acoustic standing wave may be written as

$$V'(x,t) = V_0 \cos(kx)\cos(\omega t), \tag{1}$$

where V_0 is the fluctuation amplitude, $k = \omega/c_0$ is the wave number, ω is the angular frequency, c_0 is the speed of sound and t is the time.

The interaction between the acoustic standing wave and the fluid induces the formation of steady vortex flow near the walls. A typical situation is when the characteristic length of the cavity H is far smaller than the sound wavelength λ, and far greater than the thickness of the acoustic boundary layer $\delta = \sqrt{\frac{2\nu}{\omega}}$, i.e.,

$$\delta \ll H \ll \lambda. \tag{2}$$

Using the boundary-layer theory with V_0 as small parameter [4], approximations at different orders can be obtained. The first order approximation gives the exponential decrease of the velocity V' in the acoustic boundary layer from the value given by (1) to zero at the solid walls. The second order approximation gives time-independent terms generating a steady flow in the acoustic boundary layer. This flow does not vanish outside the boundary layer, but generate a steady slip velocity [15] given by

$$V_s = v_0 \sin 2kx \quad \text{with } v_0 = \frac{3V_0^2}{8c_0}. \tag{3}$$

The velocity at the edge of the boundary layer, as given by (3), can be used as a boundary condition to determine the streaming motion. In practice, the thickness of the acoustic boundary layer can be regarded as negligible compared with the characteristic length H of the cavity, and expression (3) can then be taken as effectively a slip velocity at the solid walls. Such a boundary condition, called

boundary-velocity condition in the following, will be used in our calculations on the walls parallel to the direction x of the acoustic beam.

2.2. Governing equations

The fluid is incompressible and assumed to be Newtonian with constant kinematic viscosity and thermal diffusivity. Density variations are assumed to be linear with respect to temperature and restricted to the buoyancy term, as given by the usual Boussinesq approximation. The convective motion is then modelled by the Navier–Stokes equations coupled to an energy equation. We introduce dimensionless variables by using the following scales: H for length, H^2/ν for time, $\sqrt{Gr}\nu/H$ for velocity, $\sqrt{Gr}\rho\nu^2/H^2$ for pressure, and $(\bar{T}_h - \bar{T}_c)/A_x = \Delta\bar{T}/A_x$ for temperature. The use of A_x in the definition of the dimensionless temperature allows to define a temperature field with constant temperature gradient (the main force in the system) at diffusive state, independently of the aspect ratio A_x. The governing equations are then:

$$\nabla \cdot \vec{V} = 0 \tag{4}$$

$$\frac{\partial \vec{V}}{\partial \theta} + \sqrt{Gr}(\vec{V}\cdot\nabla)\vec{V} = -\nabla p + \nabla^2\vec{V} + \sqrt{Gr}T\vec{e}_y \tag{5}$$

$$\frac{\partial T}{\partial \theta} + \sqrt{Gr}(\vec{V}\cdot\nabla)T = \frac{1}{Pr}\nabla^2 T \tag{6}$$

where the dimensionless variables are the velocity vector $\vec{V}$, the time θ, the pressure p and the temperature T. $\vec{e}_y$ is the unit vector in the vertical direction, and the non-dimensional parameters are the Grashof number $Gr = \beta g \Delta\bar{T} H^3/(A_x\nu^2)$ and the Prandtl number $Pr = \nu/\kappa$, where ν is the kinematic viscosity and κ is the thermal diffusivity.

The thermal boundary conditions at the walls are:

$T = -A_x/2$ at the left wall, $x = 0$,
$T = +A_x/2$ at the right wall, $x = 5$,
$\partial T/\partial n = 0$ at the other walls.

No-slip condition is used at the isothermal endwalls whereas dimensionless boundary-velocity condition is used at the other walls (parallel to x) to take into account the acoustic streaming:

$V_x = V_y = V_z = 0$ at the left and right walls, $x = 0$ and $x = 5$,
$V_x = (R_s/\sqrt{Gr})\sin 2kx = Fr \sin 2kx$, $V_y = V_z = 0$ at the other walls,
where R_s is the streaming Reynolds number and Fr the acoustic Froude number, which will be discussed in Section 2.3.

Concerning the initial conditions, the numerical results obtained at a given Grashof number are successively used for the computation at a higher or lower Grashof number. This will be described in Section 2.6.

2.3. Streaming Reynolds number and acoustic Froude number

The Reynolds number expresses the ratio of the inertial forces to the viscous forces in the fluid. It is normally defined as $Re = U^* L^*/\nu$ where U^* and L^* are characteristic velocity and length. Depending on the choice of U^* and L^*, different expressions can be obtained (see Table 1). Concerning buoyancy at high Grashof number, the velocity rather evolves as $\sqrt{Gr}$, so that a good choice for Re is $Re = \sqrt{Gr}$. Concerning acoustic streaming, different streaming Reynolds number can be defined. Stuart [21] and Vainshtein [14,16] respectively used $\hat{R}_s$ and $\hat{\hat{R}}_s$, as expressed in Table 1. In our case, as we want to use the same characteristic length $L^* = H$ for both the streaming Reynolds number and the Grashof number, we define another streaming Reynolds number

$$R_s = \frac{v_0 H}{\nu} = \frac{3V_0^2 H}{8c_0\nu}, \tag{7}$$

which is introduced in the dimensionless form of the boundary-velocity condition deduced from (3).

In order to study the influence of the acoustic streaming upon the heat transfer, Vainshtein [15] introduced the acoustic Peclet number,

$$Pe = \frac{3V_0^2 H^2 \omega}{32\kappa c_0^2}, \tag{8}$$

with $V_0 = \frac{p_1}{\rho_0 c_0}$, where p_1 is the amplitude of the acoustic pressure. This choice is in fact not appropriate for comparing the relative magnitudes of acoustic streaming and thermal convection in our study, as the important parameter of thermal convection, $\Delta\bar{T}$, is not taken into account. Richardson [8] introduced the dimensionless parameter $4\hat{R}_s/\sqrt{Gr}$ in order to study the effects of sound fields on natural convection from a cylinder. We will define a similar parameter for our study, namely an acoustic Froude number Fr,

$$Fr = \frac{F_{\text{acoustic}}}{F_{\text{buoyancy}}} = \frac{R_s}{\sqrt{Gr}} = \frac{3V_0^2}{8c_0\sqrt{\beta g \Delta\bar{T} H}}. \tag{9}$$

This parameter Fr corresponds to the dimensionless form of the boundary-velocity condition. In this paper, we will consider three values of Fr: $Fr = 0$, $Fr = 0.316$ and $Fr = 0.745$.

Table 1
Dimensionless numbers according to different characteristic velocities and lengths

	L^*	U^*	Re
1	H	$\sqrt{\frac{g\beta H\Delta\bar{T}}{A_x}}$	$\sqrt{Gr} = \sqrt{\frac{g\beta\Delta\bar{T}H^3}{A_x\nu^2}}$
2	$\frac{V_0}{\omega}$	V_0	$\hat{R}_s = \frac{V_0^2}{\omega\nu}$
3	$\frac{(H/2)^2}{c_0/\omega}$	v_0	$\hat{\hat{R}}_s = \frac{3V_0^2H^2\omega}{32\nu c_0^2}$
4	H	v_0	$R_s = \frac{3V_0^2 H}{8c_0\nu}$

2.4. Nusselt number

The Nusselt number at the hot wall is calculated in order to analyze the effect of the acoustic streaming on the heat transfer:

$$Nu = \frac{-\frac{1}{\mathrm{Surf}}\int_{\mathrm{Surf}}\frac{\partial T}{\partial n}\mathrm{d}s}{-(T_\mathrm{h}-T_\mathrm{c})/A_x} = \frac{1}{\mathrm{Surf}}\int_{\mathrm{Surf}}\frac{\partial T}{\partial n}\mathrm{d}s. \quad (10)$$

The Nusselt number is 1 in the purely diffusive situation. For oscillatory flows, a mean Nusselt number is calculated by averaging its value over one period of oscillation.

We also introduce the mean fluid temperature T_fm in order to discuss changes in the structure of the thermal convection:

$$T_\mathrm{fm} = \frac{1}{\mathrm{Vol}}\int_{\mathrm{Vol}} T\mathrm{d}v. \quad (11)$$

Table 2
Tests of numerical accuracy with different meshes

	$36\times18\times16$	$36\times22\times20$	$40\times24\times22$	$44\times26\times24$
$u_{\max}$	1.252229402	1.256700524	1.263339036	1.263823667
$v_{\max}$	0.522734125	0.528474957	0.535518412	0.535315766
$w_{\max}$	0.272877955	0.272346380	0.263011611	0.272855103
Nu	1.330637874	1.330640139	1.330635961	1.330636383

Table 3
Periods and amplitude in the oscillation flow ($Fr = 0$)

Item	Period of Nu (and of T)		Amplitude of Nu	
Gr	Increase	Decrease	Increase	Decrease
53,000		0.0250(0.0499)		0.000472
54,000	0.0248(0.0495)	0.0248(0.0495)	0.001051	0.001051
56,000	0.0244(0.0488)	0.0244(0.0488)	0.002056	0.002056
58,000	0.0240(0.0480)	0.0240(0.0480)	0.003004	0.003004
59,000	0.0238(0.0476)	0.0238(0.0476)	0.003588	0.003588
60,000	0.0236(0.0472)	0.0236(0.0472)	0.004337	0.004337
62,000	0.0232(0.0465)	0.0232(0.0465)	0.006248	0.006248
63,000	0.0230(0.0461)	0.0230(0.0461)	0.007270	0.007270
64,000	0.0457(0.0457)	0.0457(0.0457)	0.010353	0.010353
66,000	0.0899(0.0899)	0.0899(0.0899)	0.016691	0.016691

Table 4
Periods and amplitude in the oscillation flow ($Fr = 0.316$)

Item	Period of Nu (and of T)		Amplitude of Nu	
Gr	Increase	Decrease	Increase	Decrease
56,000	0.1309(0.1309)	0.1309(0.1309)	0.016808	0.016808
57,000	0.1229(0.1229)	0.1229(0.1229)	0.019590	0.019590
58,000	0.1210(0.1210)	0.1210(0.1210)	0.024839	0.024839
60,000	0.1270(0.1270)	0.1270(0.1270)	0.034339	0.034339
62,000	0.1270(0.1270)	0.1273(0.1273)	0.045518	0.041869

Table 5
Periods and amplitude in the oscillation flow ($Fr = 0.745$)

Item	Period of Nu (and of T)		Amplitude of Nu	
Gr	Increase	Decrease	Increase	Decrease
56,000	0.0222(0.0444)	0.0222(0.0444)	0.001531	0.001531
58,000	0.0217(0.0433)	0.0217(0.0433)	0.006350	0.006350
60,000	0.0212(0.0424)	0.0212(0.0424)	0.010944	0.010944
62,000	0.0207(0.0414)	0.0207(0.0414)	0.015434	0.015434
64,000	0.0203(0.0405)	0.0203(0.0405)	0.019789	0.019789
65,000	0.0200(0.0400)	0.0200(0.0400)	0.021899	0.021899
66,000	0.0198(0.0396)	0.0198(0.0396)	0.023956	0.023956

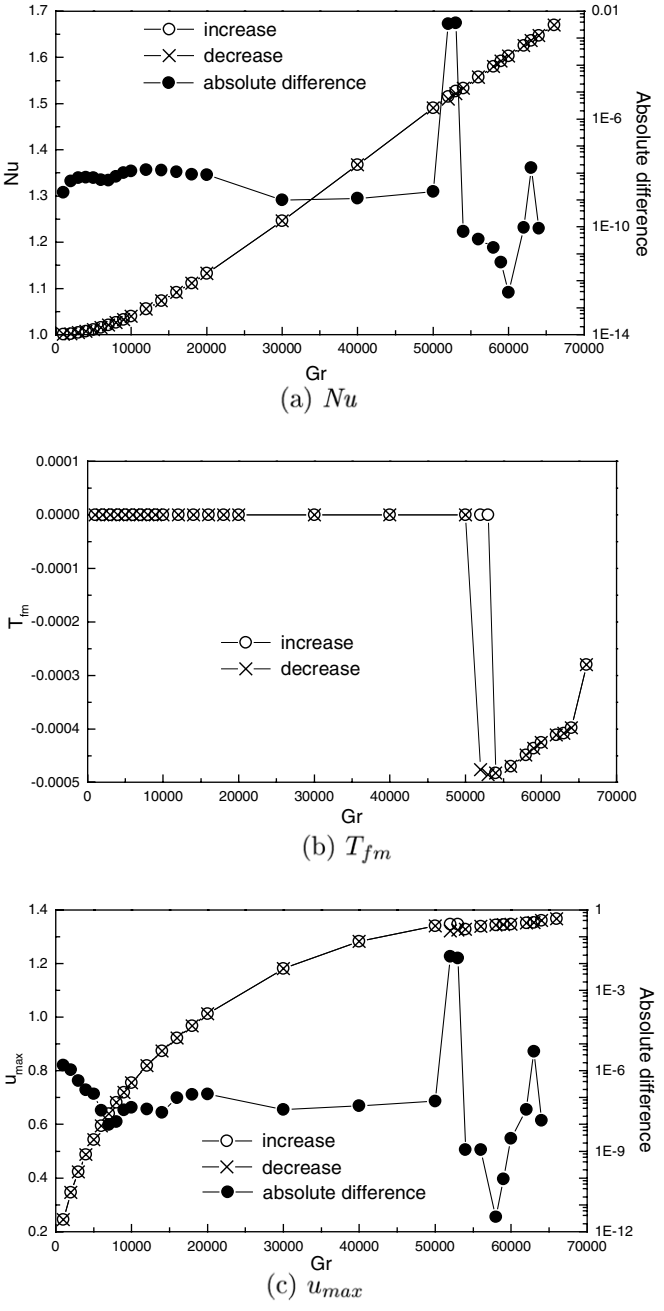

Fig. 2. Some parameters during the increase and decrease of the Grashof number ($Fr = 0$).

2.5. Numerical technique

The governing equations were solved by direct numerical simulation (DNS) with time-stepping, in a three-dimensional domain, using a spectral element method [22]. The time discretization was carried out by using the high-order splitting algorithm [23], and the spatial discretization was obtained by using Gauss–Lobatto–Legendre point distributions. All the simulations were performed with double precision arithmetic.

2.6. Computational procedure

The occurrence of hysteresis phenomena is sensitive to the thermal history, so the numerical simulations are performed by progressively increasing or decreasing the Grashof number in successive runs. The first solution is calculated from an initial purely diffusive solution corresponding to a linear temperature distribution along x and no flow. A solution obtained at Gr_{old} is then used as initial condition to solve the subsequent case at $Gr_{\text{new}} = Gr_{\text{old}} + \Delta Gr$. The step ΔGr is $\Delta Gr = 10^n$ for Grashof numbers in the range $10^n \leqslant Gr \leqslant 10^{n+1}$. Once a great change in Nusselt number or the transition from steady flow to oscillatory flow occurs, a refined step of one-fifth of the former ΔGr is employed, so as to locate the flow-transition with a better accuracy. At a bifurcation, the step is moreover halved. In this paper, the Grashof number is in the range between 1.0×10^3 and 6.6×10^4 . But in the case of $Fr = 0.316$, the oscillatory flow loses its periodicity at $Gr = 6.4 \times 10^4$, so the calculations were stopped at $Gr = 6.4 \times 10^4$ in that case.

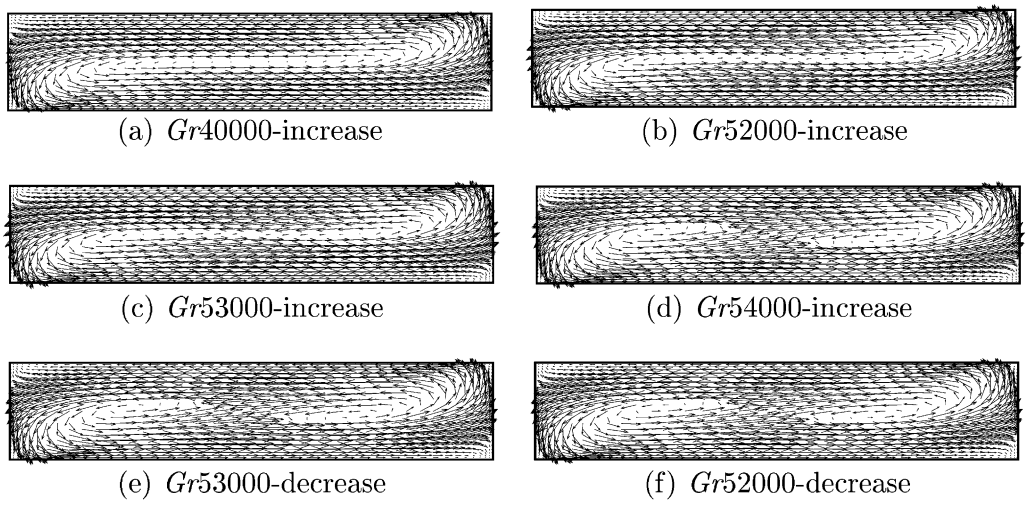

Fig. 3. Predicted fluid velocity in the P_{xy} plane in the case of $Fr = 0$.

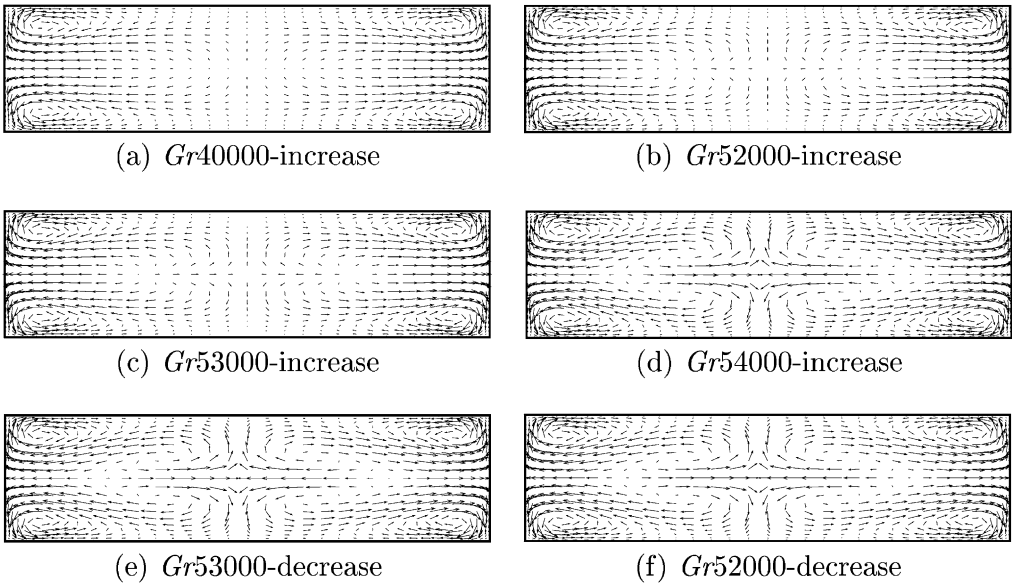

Fig. 4. Predicted fluid velocity in the P_{xz} plane in the case of $Fr = 0$.

The results are generally presented by views in the principal middle planes: the longitudinal vertical plane P_{xy}, the longitudinal horizontal plane P_{xz} and the transversal vertical plane P_{yz}, as shown in Fig. 1.

Convergence criteria and some key parameters are now given. The convergence criterion to a steady flow is based on the absolute variation ε for velocity and temperature between two adjacent time steps n and $n+1$ which at least must be less than $\varepsilon_0 = 10^{-5}$, i.e.,

$$\varepsilon = \max(|V_x^{n+1} - V_x^n|, |V_y^{n+1} - V_y^n|, |V_z^{n+1} - V_z^n|, |T^{n+1} - T^n|) < \varepsilon_0. \quad (12)$$

The Nusselt number at steady state is calculated from Eq. (10), and the maximum velocity is the absolute maximum velocity component over the whole computational domain. The convergence criterion to an oscillatory flow is based on the absolute variations for the maximum and the minimum of the Nusselt number in adjacent periods which must be less than 10^{-6}. The mean Nusselt number at the hot wall and the mean flow field are calculated by averaging the results over one period of oscillation, and the maximum velocity is the maximum value obtained over one period.

3. Validation of numerical results

To ensure that the solutions are not spurious artifacts of poorly resolved grids, grid sensitivity experiments were carried out for a steady flow calculation at $Gr = 37{,}500$ and $Pr = 0.019$. Table 2 gives the averaged Nusselt number and the maxima of the velocity components obtained on the grid nodes for four different meshes. When the grid is refined from $36 \times 18 \times 16$ to $36 \times 22 \times 20$, the maxima of the velocity components agree within 3.6%. Between the meshes $40 \times 24 \times 22$ and $44 \times 26 \times 24$, the variation of $u_{\max}$

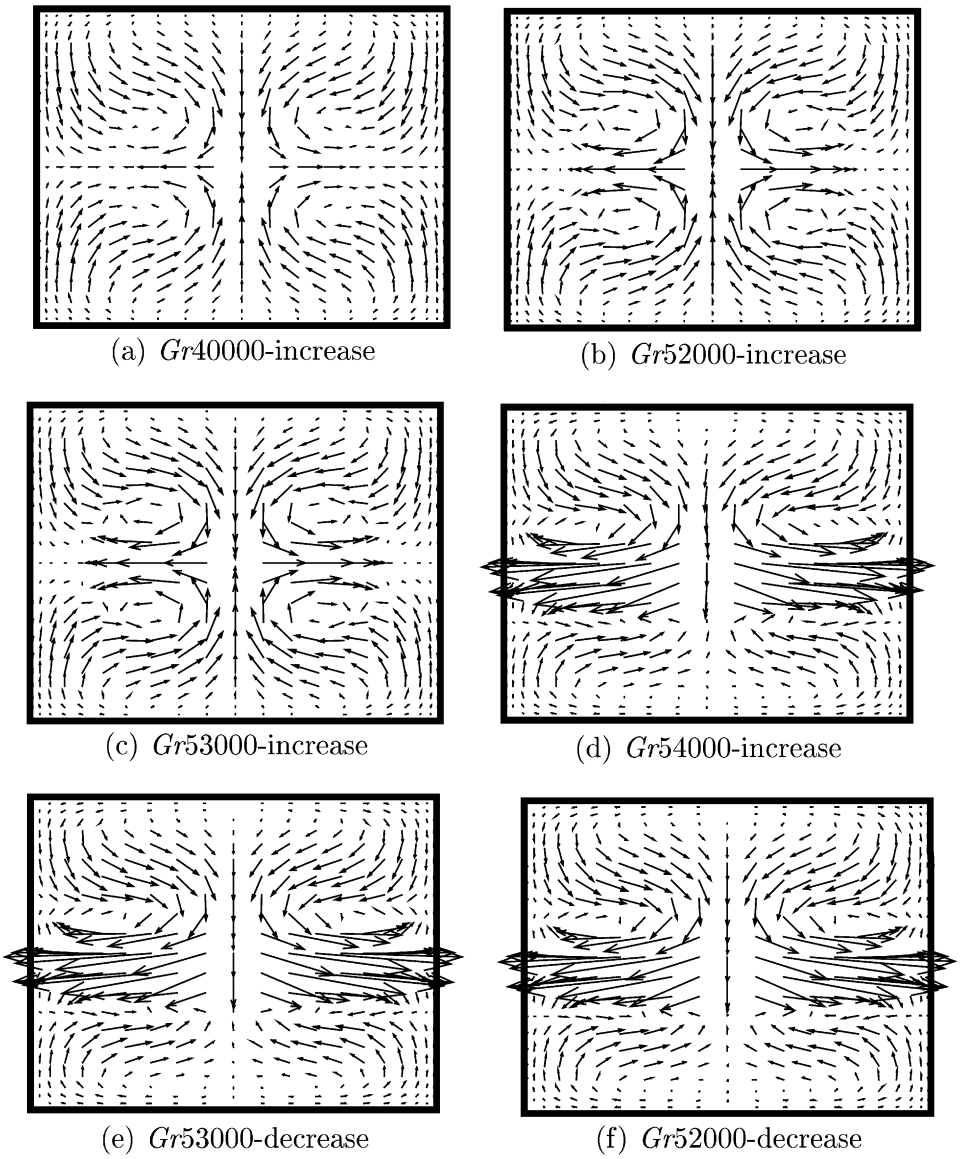

Fig. 5. Predicted fluid velocity in the P_{yz} plane in the case of $Fr = 0$.

is on the fifth digit whereas the difference on v_{max} is 0.000203, i.e., approximately 0.04%. Only w_{max} presents a larger variation, but this is connected to the change of the grid points position when the number of points in the transverse z direction is changed from 22 to 24. Due to this change of the points position with the grid refinement, there is a difficulty to judge the accuracy from the maximum velocity on the grid points. The results are in fact better than what is thus obtained. It is why it is interesting to calculate the Nusselt number which is a global quantity. When the grid is refined from $36 \times 18 \times 16$ to $44 \times 26 \times 24$, the variation of Nusselt number is on the seventh digit. And more precisely between the meshes $40 \times 24 \times 22$ and $44 \times 26 \times 24$, the variation is on the eighth digit. Therefore, the $40 \times 24 \times 22$ mesh is considered as sufficiently fine to calculate our convective flows.

4. Results and discussion

The results concerning the steady and oscillatory convective flows obtained in the differentially heated parallelepipedic cavity (with dimensions 5:1:1.3) under the influence of a Rayleigh acoustic streaming are now presented. All the numerical simulations were performed for $Pr = 0.019$. This value is taken from the experiment with gallium of Hof et al. [20]. Three levels of acoustic streaming influence will be considered corresponding to the Froude number values $Fr = 0$, $Fr = 0.316$ and $Fr = 0.745$. The oscillatory flows will be characterized by the period and the oscillation amplitude of the Nusselt number at the hot wall and by the period of the temperature at the point (3.95, 0.928, 0.0094) (see Tables 3–5). The selected point is an ordinary point, but chosen outside the symmetry planes and axes in order to avoid particular behaviours. The determination of the periods and amplitudes is directly made from the registered signals, and the accuracy is connected to the number of time steps in a period, generally around 1000. But the key parameter to analyze both the steady flows and the periodic flows will be the Nusselt number, which will be averaged for periodic flows.

Henry & Buffat [24] indicated that the steady flow solutions at low Gr in differentially heated parallelepipedic cavity contain two symmetries: one is a reflection symmetry S with respect to the P_{xy} plane (left–right symmetry), the other is a π-rotational symmetry S_r about the z'-axis shown in Fig. 1. These symmetries are defined as

$$S : (x, y, z, t) \rightarrow (x, y, A_z - z, t), (u, v, w, T) \rightarrow (u, v, -w, T)$$

and

$$S_r : (x, y, z, t) \rightarrow (A_x - x, 1 - y, z, t),$$
$$(u, v, w, T) \rightarrow (-u, -v, w, -T).$$

These symmetry properties will be checked to be valid or not for the different flows obtained, steady or oscillatory. For oscillatory flows, mainly the time-averaged flow field will be considered as in Figs. 3–5, 7–9 and 11–13. We recall that the steady flows in differentially heated cavities consist of a long convective loop going up the hot wall, along the top, down the cold wall, and back to the hot wall along the bottom. The oscillatory flows correspond either to oscillations of this loop, or to more localized oscillations inside the loop, but in any case they will strongly depend on the broken symmetries.

4.1. Fr = 0

The case $Fr = 0$ corresponds to the pure buoyancy-driven convective situation without acoustic streaming. The solutions obtained when progressively increasing and

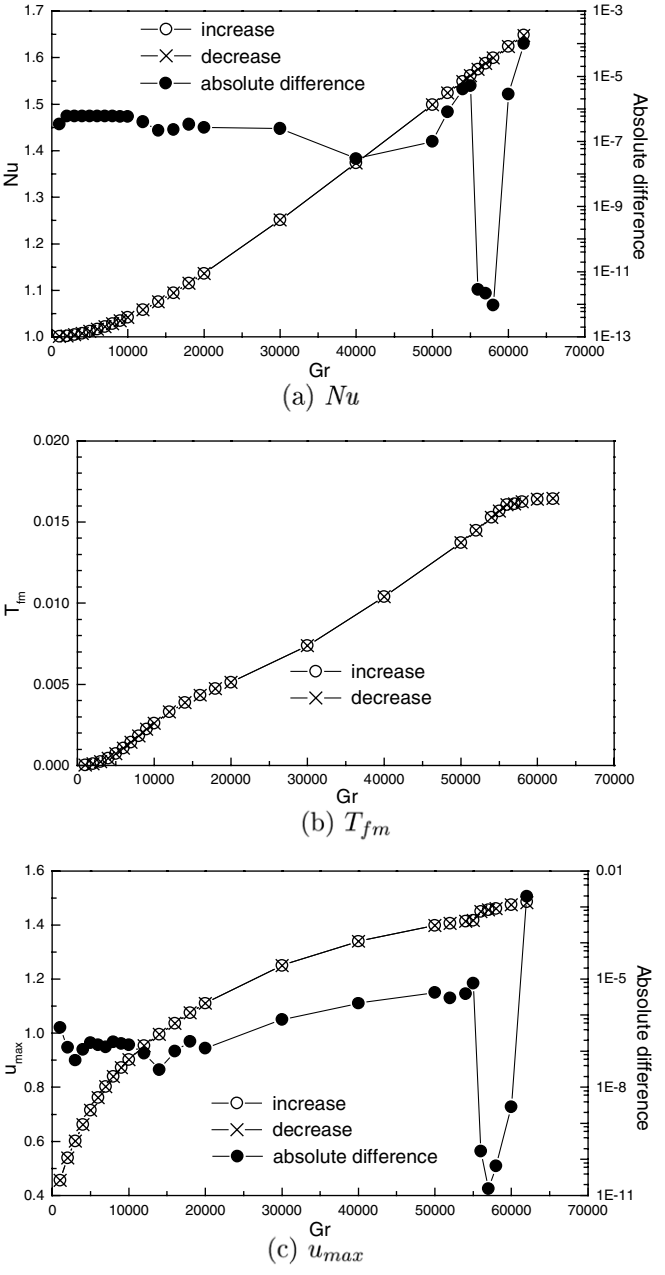

Fig. 6. Some parameters during the increase and decrease of the Grashof number ($Fr = 0.316$).

then decreasing Gr are reported in Fig. 2 and Table 3 through the evolution of different characteristics of the flow. In this figure (as in Figs. 6 and 10) are also given absolute differences between both solutions obtained at a given Gr when first increasing Gr and then decreasing it. As convergence criteria are fixed to 10^{-5}, these differences are significative (indication of two different solutions) only when they are clearly larger than this value. The Nusselt number (Fig. 2(a)) is found to increase when the Grashof number gets stronger values, reaching an almost linear evolution with Gr for $Gr > 40{,}000$. Nevertheless the evolution of the flow is not so regular as hysteresis phenomena and transition to oscillatory flows are observed. The oscillatory flow appears for $Gr = 54{,}000$ when increasing Gr whereas it disappears for $Gr = 52{,}000$ when decreasing Gr. There are then two different solutions for $Gr = 53{,}000$, a steady flow obtained for increasing Gr and an oscillatory flow obtained for decreasing Gr. The hysteresis is also present at $Gr = 52{,}000$ (Fig. 2(a)) as the steady flow obtained when decreasing Gr ($Nu = 1.510293$) is different from that obtained when increasing Gr ($Nu = 1.515512$). Some precisions on the flow are given in Fig. 2(b) through the mean fluid temperature T_{fm}. T_{fm} is zero for small Gr when all the symmetries are effective, but it becomes non-zero when the flow is oscillatory as well as for the steady state obtained for decreasing Gr at $Gr = 52{,}000$, indicating a breaking of symmetry in those cases. At last, Fig. 2(c) shows that $u_{\max}$ becomes almost constant for the larger values of Gr, indicating a variation as $\sqrt{Gr}$ for the dimensionalized velocities in this domain of Gr.

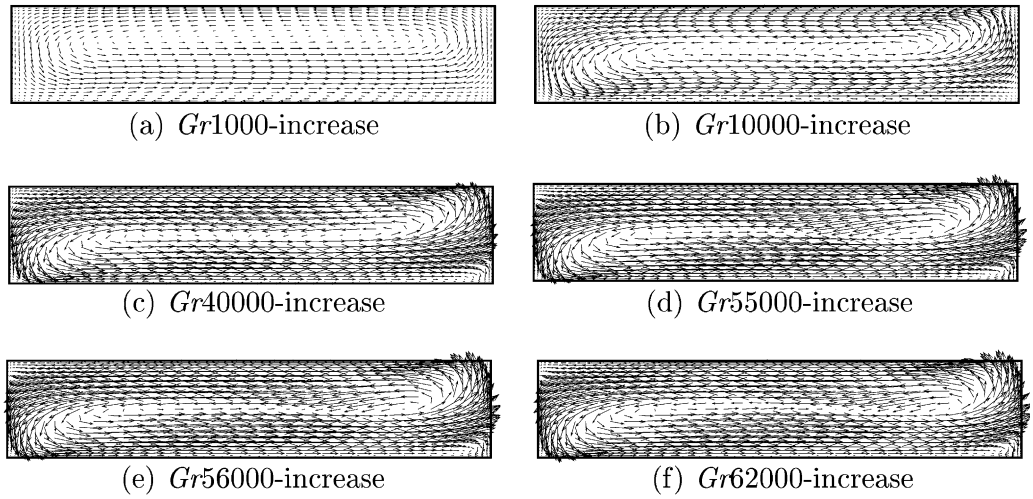

Fig. 7. Predicted fluid velocity in the P_{xy} plane in the case of $Fr = 0.316$.

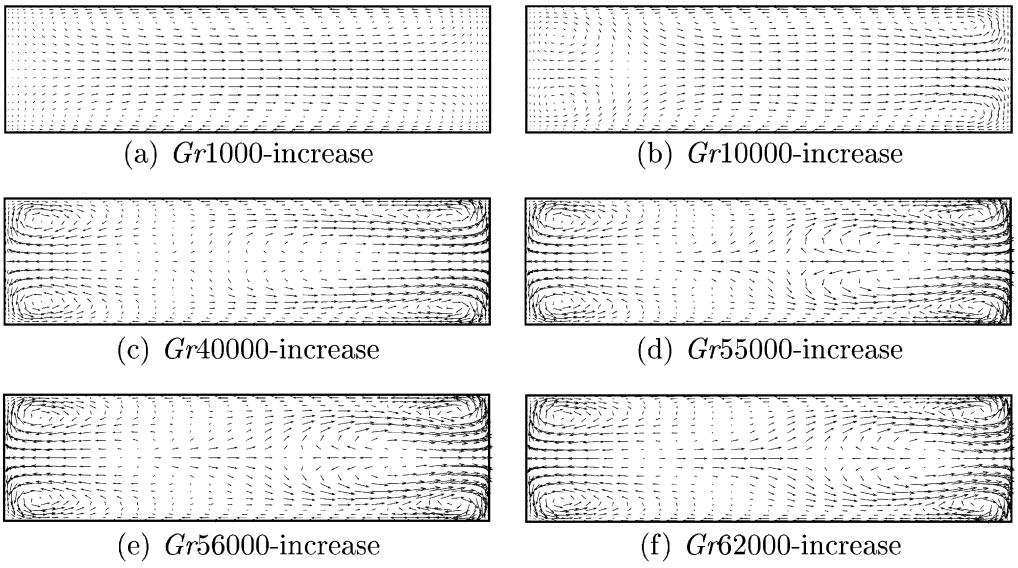

Fig. 8. Predicted fluid velocity in the P_{xz} plane in the case of $Fr = 0.316$.

Figs. 3–5 show velocity plots in the principal middle planes for selected values of Gr in order to more precisely describe the appearance and disappearance of the oscillatory flow with the hysteresis phenomenon when Gr is successively increased and decreased.

- For small Gr, due to buoyancy, the fluid motion is up the hot wall, across the top, down the cold wall and returning across the bottom. Four rolls appear at the corners in the planes P_{xz} and P_{yz}, but the fluid flow is very weak in the middle of the plane P_{xz}. The flow field, which is steady, exhibits the π-rotational symmetry S_r about the z' axis and the symmetry S with respect to the plane P_{xy}.
- When Gr is increased from 40,000 to 53,000, the flow is still steady and symmetric but some changes appear. The flow in the P_{xy} plane is less parallel inducing some velocities in the middle of the P_{xz} plane and a saddle-node point in the center of the P_{yz} plane.
- When Gr is increased between 54,000 and 58,000, the flow becomes oscillatory. In fact this transition is very slow and the solution first evolves to a steady flow with a good convergence criterion ($\varepsilon < 10^{-8}$) before becoming oscillatory. The time-averaged flow shown in Figs. 3(d), 4(d) and 5(d), presents now a strong interaction between the two reverse flows in the center of the cavity visible in the three main middle planes. Fig. 5(d) also shows that the symmetry S_r is broken for the time-averaged flow, but that the symmetry S is still maintained. For this oscillatory flow, as shown in Table 3, the period measured on temperature is two times that obtained for the Nusselt number. The period decreases with the increase of the Grashof number, whereas the amplitude increases.

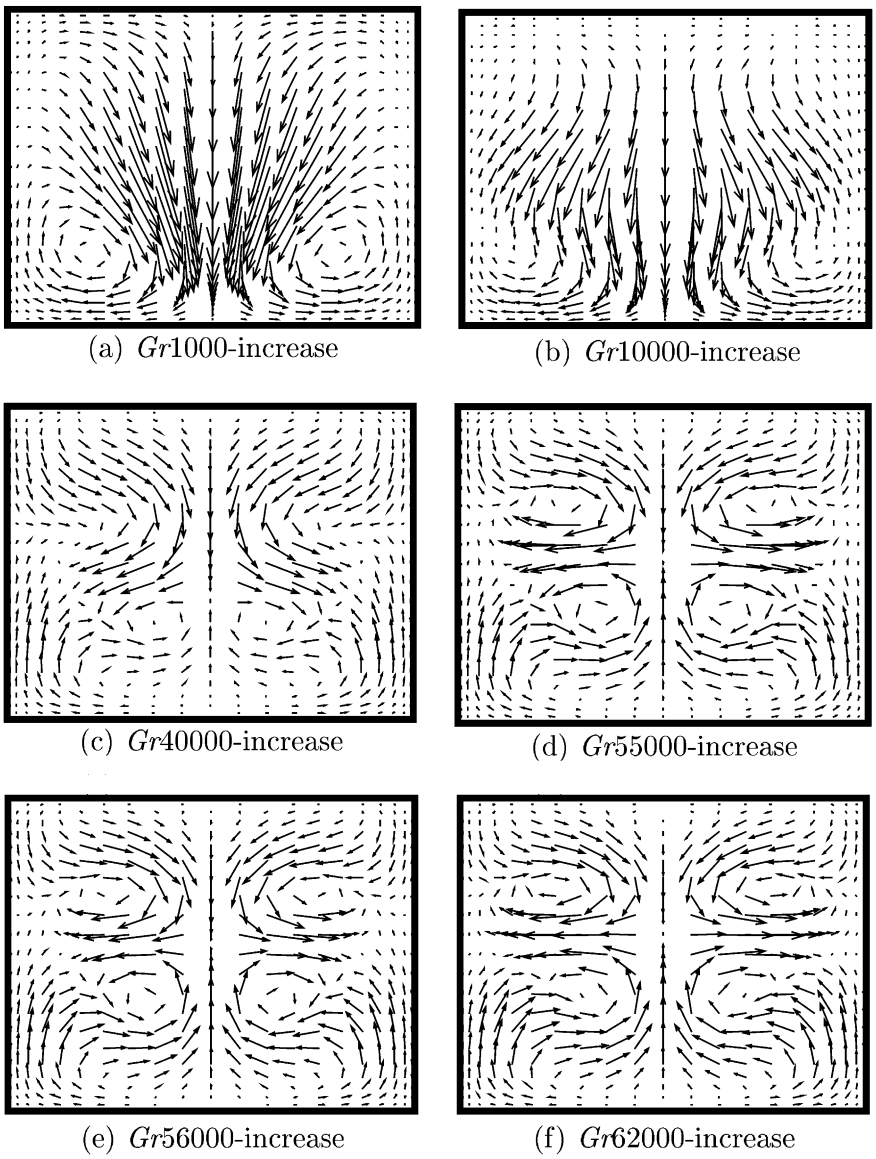

Fig. 9. Predicted fluid velocity in the P_{yz} plane in the case of $Fr = 0.316$.

– When the Grashof number is greater than 64,000, the period for *Nu* becomes equal to that for temperature. When the Grashof number is up to 66,000, a period doubling occurs.
– When *Gr* decreases from 59,000 to 54,000, the flow still remains periodic, with periods and amplitudes equal to that in the *Gr*-increasing course, as shown in Table 3. But this oscillatory flow still exists for *Gr* down to 53,000, which is different from what was observed in the *Gr*-increasing course (steady flow).
– When *Gr* is about 52,000, the flow changed from oscillatory to steady. But this solution is different from that obtained in the *Gr*-increasing course as there is still a strong interaction between the two reverse flows in the center of the cavity and the symmetry S_r of the flow is still broken, as shown in Figs. 3(f), 4(f) and 5(f).
– When *Gr* is down to 50,000, the symmetry S_r is recovered, and along the further decrease of the Grashof number, the flow is the same as that in the *Gr*-increasing course.

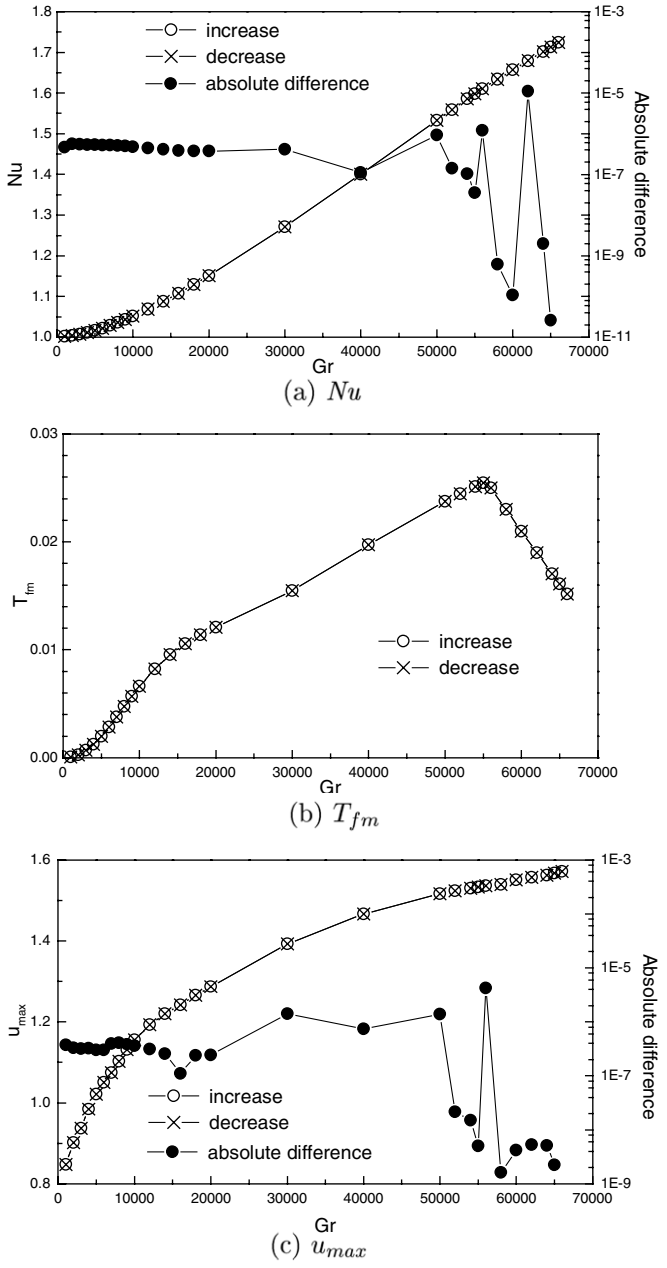

Fig. 10. Some parameters during the increase and decrease of the Grashof number ($Fr = 0.745$).

4.2. $Fr = 0.316$

The case $Fr = 0.316$ corresponds to a situation with combined buoyancy-driven convection and acoustic streaming. The solutions obtained when progressively increasing and then decreasing *Gr* are reported in Fig. 6 and Table 4. Table 4 shows that the oscillatory flow appears for $Gr = 56{,}000$ for increasing *Gr* and disappears at the same level for decreasing *Gr*. Moreover, Fig. 6 shows that there is only one solution for the steady flow or the oscillatory flow if $Gr \leqslant 60{,}000$ because the different quantities as the Nusselt number and maximum velocity are the same during the increase and decrease of *Gr*. This is the indication that no hysteresis occurs in this case. In fact, Table 4 shows that some differences occur in the case $Gr = 62{,}000$ when increasing or decreasing *Gr*, indicating that there are different oscillatory solutions in this case.

Figs. 7–9 show the sequences of the onset, development and vanishing of the oscillatory flow under sound field when increasing and decreasing the Grashof number.

– Figs. 7(a) and 8(a) show that for $Gr = 1000$ two rolls appear in the P_{xy} and P_{xz} planes, reminiscent of the pure acoustic streaming flow. In the P_{xy} plane, the upper roll is reinforced by the buoyancy flow and then bigger than the bottom roll. As shown in Fig. 9(a), due to the acoustic streaming, the flow does not satisfy any more the π-rotational symmetry S_r about the z' axis. But at $Gr = 1000$, the symmetry *S* about the P_{xy} plane is well satisfied.
– At $Gr = 10{,}000$, the buoyancy roll is clearly dominant in the P_{xy} plane (Fig. 7(b)), acoustic streaming having still an influence in this plane close to the boundaries, and in the P_{xz} plane (8(b)).
– With the increase of the Grashof number, the classical four rolls of the buoyancy flow in the P_{xz} plane clearly appear (8(c)). The flow is also less parallel in the middle of the P_{xy} plane than without acoustic streaming (7(c)).
– The oscillatory flow occurs when the Grashof number is increased up to 56,000. The time-averaged flow field at this value is quite similar to the steady flow obtained at $Gr = 55{,}000$ indicating a continuity between the steady and oscillatory states. This time-averaged fluid flow still keeps the symmetry *S* about the P_{xy} plane, as shown in Figs. 8(f) and 9(f). Table 4 shows a clear increase of the amplitudes and a slight variation of the period for the Nusselt number when the Grashof number is changed from 56,000 to 62,000.

– When the Grashof number is up to 64,000, a non-periodic flow occurs. And when Gr is decreased to 62,000, a periodic flow is recovered, but different from that obtained when increasing Gr, as shown by the different periods and amplitudes for the Nusselt number given in Table 4.
– For smaller Gr values, the solutions calculated are similar to that obtained when increasing Gr.

4.3. $Fr = 0.745$

The case $Fr = 0.745$ corresponds to a stronger influence of acoustic streaming. The solutions obtained when progressively increasing and then decreasing Gr are reported in Fig. 10 and Table 5. Table 5 shows that the oscillatory flow appears at $Gr = 56{,}000$ for increasing Gr and disappears at the same level for decreasing Gr. Fig. 10 shows that in this case a single solution is obtained for a given Grashof number at least up to $Gr = 66{,}000$.

Figs. 11–13 show the sequence of the onset, development and vanishing of oscillatory flow with the increase and decrease of the Grashof number. Except for $Gr = 1000$ and 10,000 where the influence of acoustic streaming is more clearly seen than for $Fr = 0.316$, the flow field is generally very similar to that obtained for $Fr = 0.316$, which can explain the comparable values

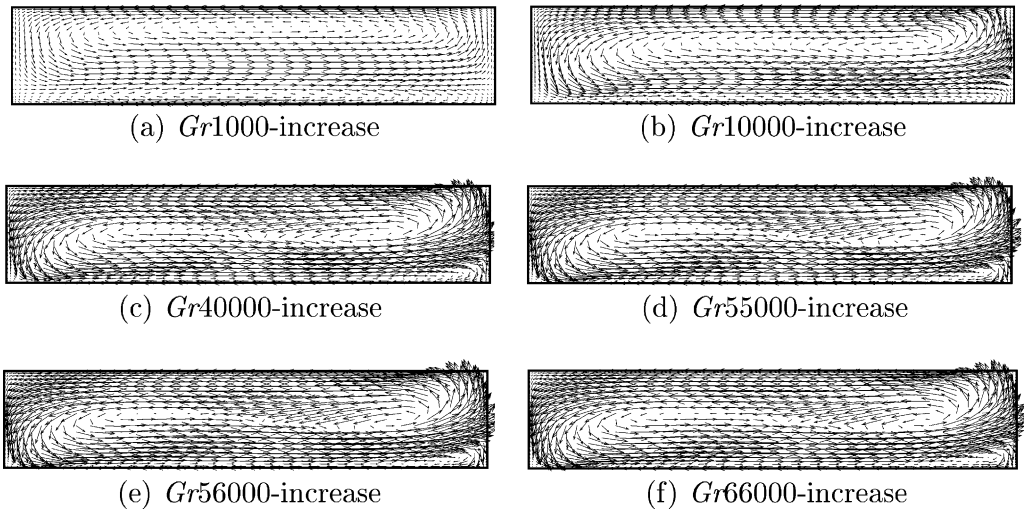

Fig. 11. Predicted fluid velocity in the P_{xy} plane in the case of $Fr = 0.745$.

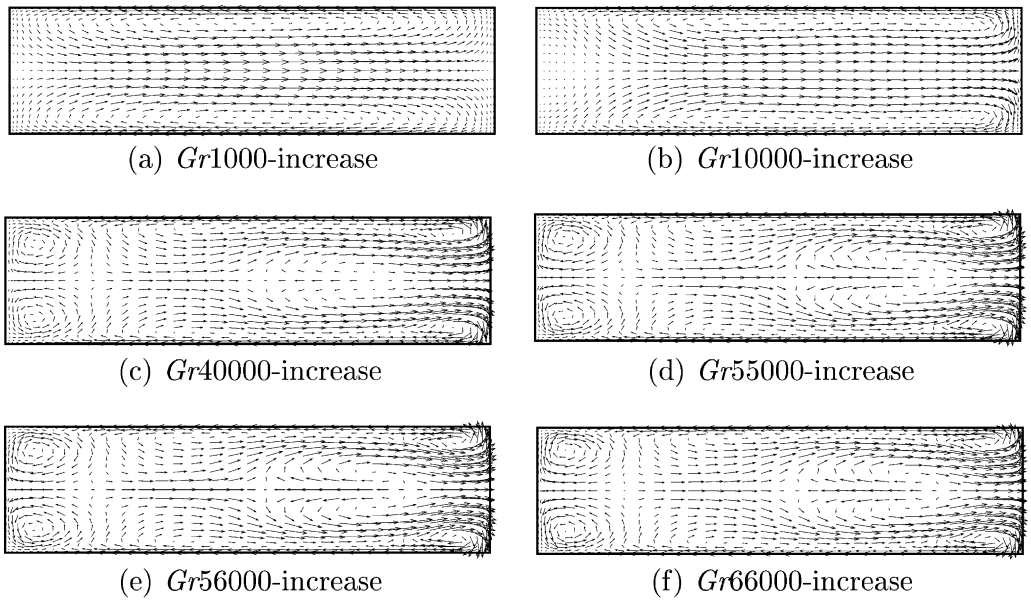

Fig. 12. Predicted fluid velocity in the P_{xz} plane in the case of $Fr = 0.745$.

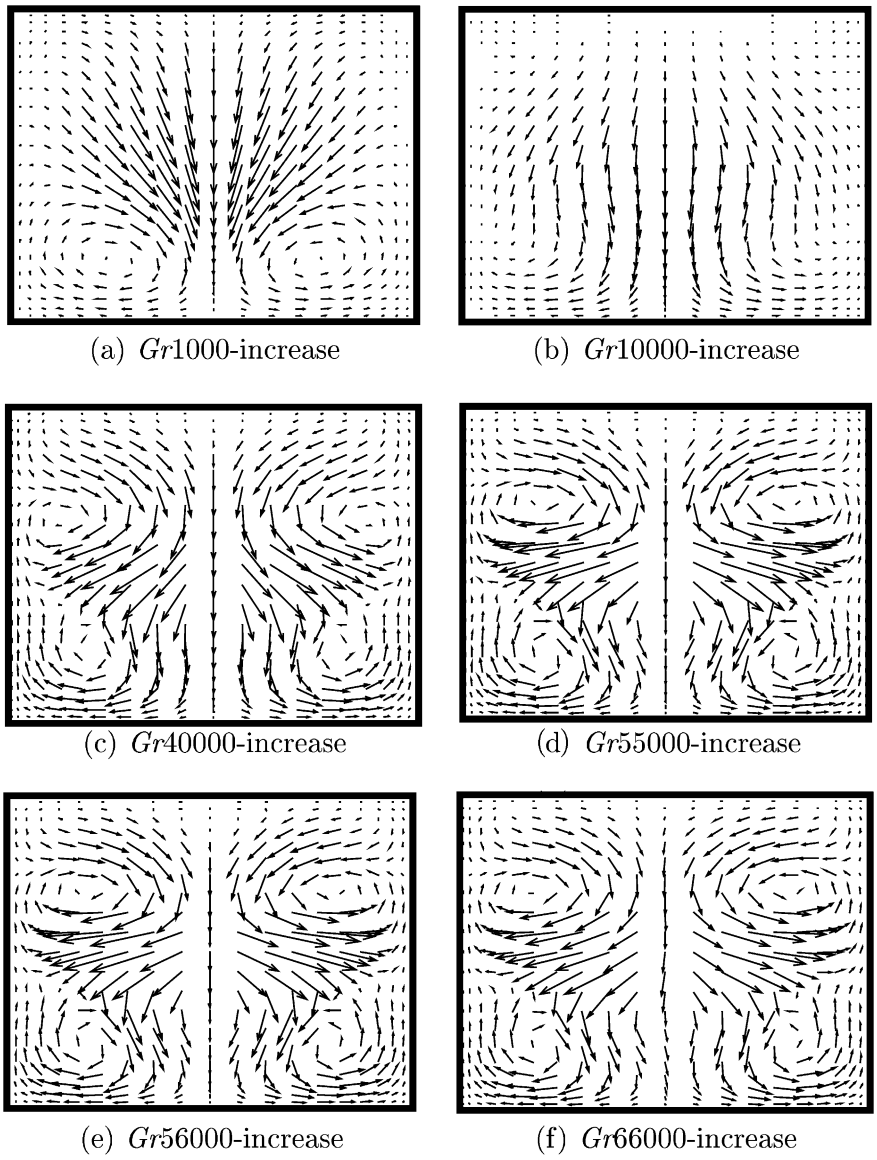

Fig. 13. Predicted fluid velocity in the P_{yz} plane in the case of $Fr = 0.745$.

obtained for the transition to oscillatory states. In fact this oscillatory transition is very slow for $Fr = 0.745$ with a first evolution to a steady flow before the triggering of oscillations, as was already observed for $Fr = 0$.

4.4. General discussion

Fig. 14 shows the instantaneous oscillatory flow field in the three cases, $Fr = 0$, $Fr = 0.316$ and $Fr = 0.745$. In any case, we have seen that the symmetry S with respect to the P_{xy} plane was effective for the time-averaged flow field. From Fig. 14, we see that this symmetry S is also effective in the instantaneous velocity field for $Fr = 0.316$, but is lost in the instantaneous velocity field for $Fr = 0$ and $Fr = 0.745$. This feature can explain the differences found on the period of the Nusselt number compared to that of the temperature. When no symmetry is broken ($Fr = 0.316$), the Nusselt number continuously changes during an oscillatory sequence. But when the symmetry S is broken, two states distant by half an oscillatory sequence are the symmetric of each other, and correspond then to the same value of Nu. This explains why the period for Nu is half the global period of the flow in these cases.

Concerning the transition from steady flow to oscillatory flow, hysteresis phenomenon occurs for $Fr = 0$, but no hysteresis was found for $Fr = 0.316$ and $Fr = 0.745$. Schematic bifurcation diagrams for the different cases are given in Fig. 15 (the solid lines denote the stable states and the dashed lines the unstable states). Detailed analysis of the numerical calculations shows three kinds of transitions for $Fr = 0$. The first is a transition from a S and S_r symmetric steady flow directly to an oscillatory flow at $Gr = 54{,}000$ by a stepwise increase of Grashof number. This oscillatory flow has lost all the symmetries, but for time-averaged quantities, only the symmetry S_r is broken whereas the symmetry S is maintained. The second transi-

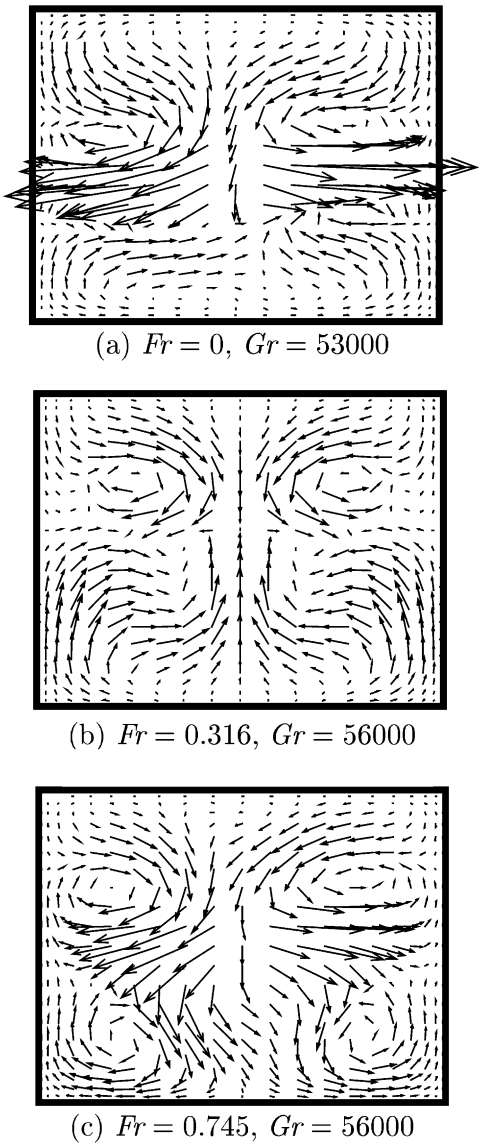

Fig. 14. Instantaneous flow in the P_{yz} plane for the three oscillatory cases.

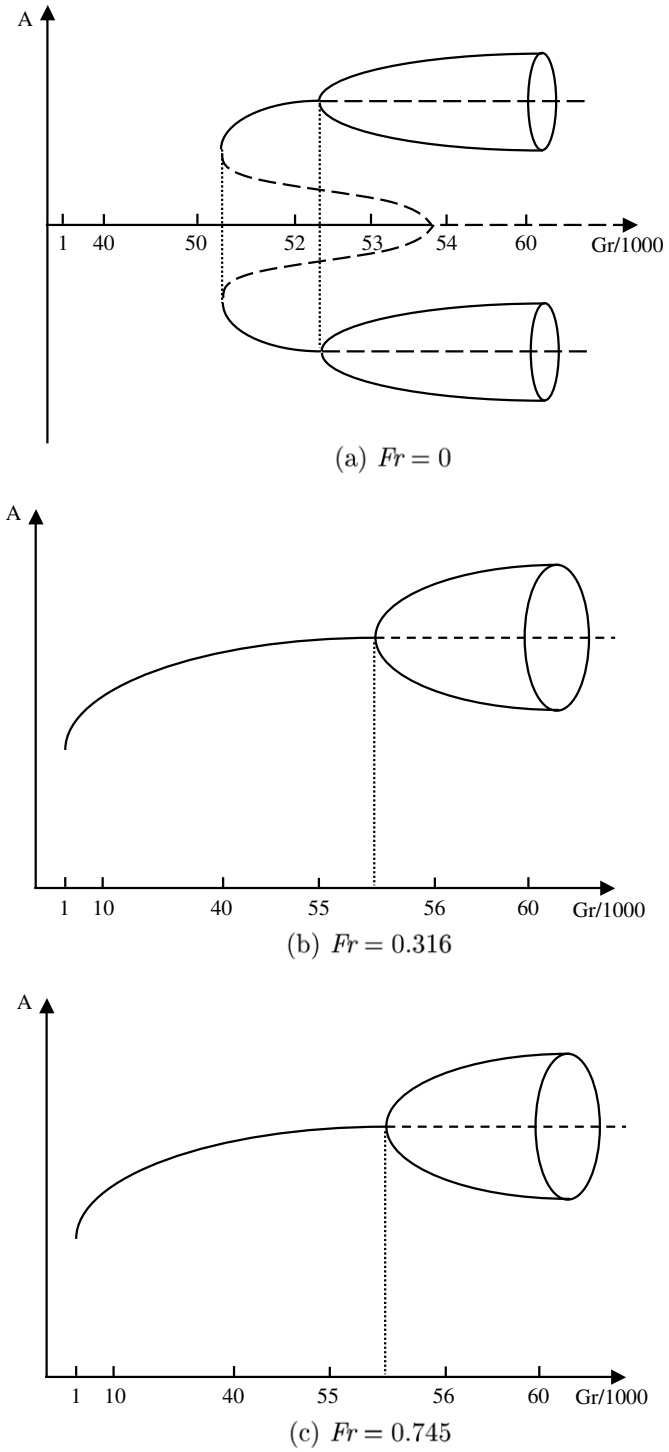

Fig. 15. Schematic bifurcation diagram for the onset of oscillations.

tion is a transition from the oscillatory flow to a S symmetric steady flow at $Gr = 52{,}000$ when decreasing Gr. The last transition is a transition from a S symmetric steady flow to the S and S_r symmetric steady flow at $Gr = 50{,}000$ when decreasing Gr. From these observations, a possible scenario for the transitions would be the existence of a first sub-critical S_r-symmetry-breaking steady bifurcation and a super-critical S-symmetry-breaking Hopf bifurcation on the S_r-asymmetric branches, as shown in Fig. 15(a). Fig. 2(b) shows the variation of the mean fluid temperature T_{fm} for $Fr = 0$. The mean fluid temperature is zero for the S and S_r symmetric steady flows, in relation with these symmetries. Once the oscillatory flow occurs, T_{fm} is abruptly decreased. This phenomenon occurs because, due to the breaking of the S_r symmetry, the center of the flow field is a little displaced from the center of the cavity towards the cold wall, as shown in Figs. 4(d) and (e). An increase of T_{fm} could be obtained on the other oscillatory branch sketched in Fig. 15(a). Indeed, for this branch the breaking of the S_r symmetry is expected to move the center of the flow towards the hot wall. We can remark that $|T_{fm}|$ is decreased when further increasing Gr due to the efficient mixing related to the oscillatory state.

When the sound field is applied ($Fr \neq 0$), the boundary-velocity condition breaks the S_r symmetry which cannot be observed in the flow fields. The steady flows then have only the symmetry S with respect to the plane P_{xy}. In the two

cases ($Fr = 0.316$ and $Fr = 0.745$), the transition to oscillatory flow occurs directly on this branch, at a super-critical Hopf bifurcation which is located between 55,000 and 56,000. But for $Fr = 0.316$, this transition occurs without breaking of symmetry, whereas for $Fr = 0.745$, the transition breaks the remaining S symmetry (Figs. 15(b) and (c)).

Figs. 7 and 11 show that the acoustic streaming enhances the upper flow of hot fluid and weakens the lower flow of cold fluid. And the greater is the Grashof number, the stronger is the effect of the acoustic streaming because all the cases are conducted with a constant acoustic Froude number. This induces an increase of the mean fluid temperature T_{fm} with the increase of the Grashof number during the steady-flow stage. Once the oscillatory flow occurs, it induces a phenomenon of mixing which tends to make temperature more uniform in the cavity. In the case $Fr = 0.316$, this mixing effect seems not very efficient as only a slowdown of the increase of T_{fm} with Gr is observed. But for $Fr = 0.745$, the mixing effect is more efficient and induces a clear decrease of T_{fm}. The differences observed can be connected to the fact that for $Fr = 0.745$ the oscillatory flow occurs with the breaking of the S symmetry which induces more perturbations in the flow and makes the mixing more efficient. Such an influence of the oscillatory flow on T_{fm} was also observed for $Fr = 0$, a case where the breaking of the S symmetry at the oscillatory transition is also effective.

This study is a first step in determining the influence of an acoustic field on natural convection in a cavity. It would be interesting in the future to change the size of the cavity. Moreover, as the action of the acoustic field is independent of the electrically conducting nature of the fluid, it could be also applied to the growth of other materials such as transparent materials with different values of Pr. How these modifications of A_x, A_z, and Pr will change the action of the acoustic field on convection? A sound answer to this question cannot be given, particularly when we know that the flow transitions in heated confined cavities strongly depend on all these parameters (Wakitani [25]).

5. Conclusion

The natural convection in a differentially heated rectangular enclosure under different acoustic fields has been investigated numerically by progressively increasing and then decreasing the Grashof number. The acoustic Froude number Fr was introduced in order to quantify the effect of the acoustic streaming on the thermal convection. Without acoustic influence ($Fr = 0$), the transition to oscillatory flow only occurs after a first steady bifurcation with breaking of the π-rotational symmetry S_r, and this leads to hysteresis phenomena. With acoustic effects ($Fr \neq 0$), the S_r symmetry does not exist in the flow, leading to the disappearance of the steady bifurcation and of the hysteresis, and the oscillatory transition is then the first transition. The threshold for the oscillatory transition is increased when $Fr \neq 0$, indicating a stabilizing influence of the acoustic field. This transition occurs for $Fr = 0$ with breaking of the symmetry S with respect to the P_{xy} plane. This is also the case for $Fr = 0.745$, but not for $Fr = 0.316$. This breaking of the S symmetry induces particular effects: the period of the Nusselt number is half the main period of the flow, and the mean fluid temperature is found to decrease with the increase of Gr indicating a better mixing of the flow in this case.

Future orientations of the research will be focused on the action of the Eckart streaming, with in mind both the stabilization of heated flows for material processing applications and the increase of heat transfer for cooling devices.

Acknowledgements

The calculations were carried out on a NEC-SX5 computer with the support of the CNRS through the 'Institut du développement et des ressources en informatique scientifique'.

References

[1] S.J. Lighthill, Acoustic streaming, J. Sound Vib. 61 (3) (1978) 391–418.
[2] N. Riley, Acoustic streaming, Theoret. Comput. Fluid Dyn. 10 (1998) 349–356.
[3] J.W.S. Rayleigh, second ed. The Theory of Sound, vol. 2, Dover Publications, New York, 1945.
[4] H. Schlichting, Boundary-layer Theory, seventh ed., McGraw-Hill, New York, 1979.
[5] P.J. Westervelt, The theory of steady rotational flow generated by a sound field, J. Acoust. Soc. Am. 25 (1) (1953) 60–67.
[6] M.P. Arroyo, C.A. Greated, Stereoscopic particle image velocimetry, Meas. Sci. Technol. 2 (1991) 1181–1186.
[7] M. Campbell, J.A. Cosgrove, C.A. Greated, S. Jack, D. Rockliff, Review of LDA and PIV applied to the measurement of sound and acoustic streaming, Opt. Laser Technol. 32 (2000) 629–639.
[8] P.D. Richardson, Local effects of horizontal and vertical sound fields on natural convection from a horizontal cylinder, J. Sound Vib. 10 (1) (1969) 32–41.
[9] H. Matsumura, The influence of sound on natural convection from vertical flat plates, Int. J. Heat Mass Transfer 26 (5) (1983) 790–792.
[10] H. Engelbrecht, L. Pretorius, The effect of sound on natural convection from a vertical flat plate, J. Sound Vib. 158 (2) (1992) 213–218.
[11] N. Kawahara, A.L. Yarin, G. Brenn, O. Kastner, F. Durst, Effect of acoustic streaming on the mass transfer from a sublimating sphere, Phys. Fluids 12 (4) (2000) 912–923.
[12] A. Gopinath, D.R. Harder, An experimental study of heat transfer from a cylinder in low-amplitude zero-mean oscillatory flows, Int. J. Heat Mass Transfer 43 (2000) 505–520.
[13] G. De Vahl Davis, P.D. Richardson, Natural convection in a sound field giving large streaming Reynolds numbers, Int. J. Heat Mass Transfer 16 (1973) 1245–1265.
[14] P. Vainshtein, Rayleigh streaming at large Reynolds number and its effect on shear flow, J. Fluid Mech. 285 (1995) 249–264.
[15] P. Vainshtein, M. Fichman, C. Gutfinger, Acoustic enhancement of heat transfer between two parallel plates, Int. J. Heat Mass Transfer 38 (10) (1995) 1893–1899.
[16] P. Vainshtein, C. Gutfinger, D. Pnueli, Ignition of fuel mixtures by standing acoustic wave, Combust. Flame 118 (1999) 370–380.
[17] A.K.H. Chu, Stability of acoustic streaming flows in plane channels, Phys. Rev. E 68 (046305) (2003) 1–6.

[18] G.N. Kozhemyakin, V.G. Kosushkin, S.Y. Kurochkin, Growth of Ga–As crystals pulled under the presence of ultrasonic vibrations, J. Crystal Growth 121 (1992) 240–242.
[19] G.N. Kozhemyakin, Influence of ultrasonic vibrations on the growth of In–Sb crystals, J. Crystal Growth 149 (1995) 266–268.
[20] B. Hof, A. Juel, T. Mullin, Magnetohydrodynamic damping of convective flows in molten gallium, J. Fluid Mech. 482 (2003) 163–179.
[21] J.T. Stuart, Double boundary layers in oscillatory viscous flow, J. Fluid Mech. 24 (4) (1966) 673–687.
[22] H. BenHadid, D. Henry, Numerical study of convection in the horizontal Bridgman configuration under the action of a constant magnetic field. Part 2. Three-dimensional flow, J. Fluid Mech. 333 (1997) 57–83.
[23] G.E. Karniadakis, M. Israeli, S.A. Orszag, High-order splitting methods for the imcompressible Navier–Stokes equations, J. Comput. Phys. 97 (2) (1991) 414–443.
[24] D. Henry, M. Buffat, Two and three-dimensional numberical simulations of the transition to oscillatory convection in low-Prandtl number fluid, J. Fluid Mech. 374 (1998) 145–171.
[25] S. Wakitani, Numerical study of three-dimensional oscillatory natural convection at low Prandtl number in rectangular enclosures, J. Heat Transfer 123 (2001) 77–83.